NACA TN 3100

NATIONAL ADVISORY COMMITTEE FOR AERONAUTICS

TECHNICAL NOTE 3100

STATISTICAL STUDY OF TRANSITION-POINT FLUCTUATIONS IN SUPERSONIC FLOW

By J. C. Evvard, M. Tucker, and W. C. Burgess, Jr.

Lewis Flight Propulsion Laboratory
Cleveland, Ohio

Washington
March 1954

NATIONAL ADVISORY COMMITTEE FOR AERONAUTICS

TECHNICAL NOTE 3100

STATISTICAL STUDY OF TRANSITION-POINT FLUCTUATIONS IN SUPERSONIC FLOW

By J. C. Evvard, M. Tucker, and W. C. Burgess, Jr.

SUMMARY

The random movement of the transition point on a 10° cone at a free-stream Mach number of 3.12 was investigated by means of a large number of high-speed schlieren photographs. The distribution functions which statistically define the transition-point location were determined for a range of test-section Reynolds number and two levels of free-stream turbulence intensity. The intensity was varied by changing tunnel settling-chamber configurations. Temperature-recovery-factor distributions were also obtained.

The axial extent of the distribution function determined from the schlieren data increased with turbulence level. The axial spread of the transition region denoted by the recovery-factor measurements roughly corresponded to that of the appropriate distribution function.

These data suggest that a relatively sharp transition from laminar to turbulent flow takes place and that this flow pattern moves randomly along the aerodynamic surface. With the use of the statistical distribution functions obtained from the data and surface temperatures (as time-averaged by the surface thermocouples), the instantaneous surface-temperature distributions were calculated for two Reynolds numbers.

INTRODUCTION

Transition on an aerodynamic surface refers to that region between the laminar and fully turbulent regions of the boundary-layer flow. Transition is affected by Reynolds number, Mach number, stream turbulence, heat transfer, surface roughness, surface curvature, and pressure gradient. For transonic and supersonic flows, the effects of incident shock waves must also be considered.

The Tollmien-Schlichting theory of laminar-boundary-layer stability (ref. 1) as extended by Lees and Lin (see refs. 2 and 3) has been proposed as a mechanism leading eventually to the onset of transition, provided that the stream turbulence is sufficiently low. In a flow field for which the stream-turbulence intensity is below about 0.1 percent, very small disturbances that are always present in a laminar boundary layer will be selectively amplified according to frequency, if the flow Reynolds number is sufficiently high, until large oscillations are developed. These large oscillations, which cannot be treated by the linearized theory, lead to breakdown of the laminar flow and to transition. For turbulence intensities greater than from 0.5 to 1.0 percent in low-speed flows, the Tollmien-Schlichting waves presumably play a minor role compared with that of local adverse pressure gradients associated with the stream turbulence in promoting transition - a theory advanced by G. I. Taylor (ref. 4) wherein both intensity and scale of turbulence are considered.

The actual sequence of events in the transition process starting from breakdown of the laminar flow and culminating in establishment of fully turbulent flow is not yet known. Hugh L. Dryden has made the tentative suggestion that transition is always initiated by a separated boundary layer and that the separation may be intermittent and local in character. This separation could result from either the Tollmien-Schlichting waves or the local adverse pressure gradients suggested by Taylor. A plausible transition sequence would thus be that the separated boundary layer rolls up into discrete vortices of scale comparable to the thickness of the layer. These vortices break up and diffuse rapidly to form turbulent flow, as in the investigation of mixed periodic-turbulent phenomena reported in reference 5. Such considerations might lead one to expect a fairly rapid change from laminar to turbulent flow and, in view of the intermittent and local nature of the separated boundary-layer formation, a random longitudinal movement of the transition-point location. An alternative view is suggested by Emmons and Bryson in references 6 and 7, wherein transition is treated as a random process by postulating the sudden and random appearance in the flow field of turbulent "spots." These turbulent spots or sources grow with time and eventually join to form a fully turbulent region.

The experimental distributions of recovery factor (refs. 8 and 9) and local skin-friction coefficient (ref. 10) seemingly imply that the change from laminar to turbulent flow is a gradual one. On the other hand, high-speed schlieren photographs obtained in wind tunnels (about 1 microsec exposure) of boundary-layer development in supersonic flow suggest that the transition process must take place very quickly.

The apparent conflict between the sharply defined transition point observed on schlieren photographs and the relatively broad transition region obtained in measurements of time-averaged quantities such as recovery factor may be resolved by considering that the transition-point location may fluctuate with time. Experimental evidence is included in references 11 to 13 which demonstrates that such fluctuations do occur on models tested in supersonic wind tunnels.

In order to explore this question in greater detail, a study of transition on a thin-walled stainless-steel 10° cone at a stream Mach number of 3.12 was made with both schlieren and surface-temperature measurement techiques. The statistical distribution of transition-point location was determined by means of a uniformly timed series of high-speed schlieren photographs. Temperature distributions were obtained concurrently from surface thermocouples mounted along a ray of the same cone. The measured surface temperatures and statistical distribution functions were utilized to calculate the shape of a hypothesized instantaneous surface-temperature distribution. These investigations, which were limited to studies of the effects of Reynolds number and stream turbulence, were conducted at the NACA Lewis laboratory during the spring and summer of 1953.

APPARATUS AND PROCEDURE

Four tests were conducted in the Lewis 1- by 1-foot supersonic wind tunnel, which is a continuous-flow, nonreturn, variable-pressure tunnel operating at a Mach number of 3.12 with the specific humidity sufficiently low (about 4×10^{-5} lb of water/lb of dry air throughout most of any given run) to minimize condensation effects. Two cylindrical settling-chamber configurations were used to vary the stream-turbulence level.

In the original tunnel configuration (designated A), the flow entered parallel to the settling-chamber axis, which was transverse to the tunnel-nozzle axis. A screen having a pressure drop of $8q$ (where q designates local stream dynamic pressure) was located in the settling chamber, and a screen with pressure drop of $2q$ was placed at the exit of the settling chamber. Measurements of the longitudinal turbulence intensity were made at the Mach number 0.12 station upstream of the throat with a hot-wire probe employing tungsten wire 0.0002 inch in diameter and 0.080 inch long. An intensity of 9.4 percent was obtained for test 1. Because configuration A resulted in a high turbulence level, the settling chamber was replaced. In the revised tunnel configuration (B), the entrance-air direction and settling-chamber axis were parallel to the nozzle axis in order to achieve a straight-through flow. Four damping screens having an over-all pressure drop of $10q$ were placed in the settling chamber. A honeycomb was also installed

upstream of the screens. For configuration B, measurements of the longitudinal turbulence intensity were also made at the Mach number 0.12 station, yielding intensities of 1.0, 0.75, and 0.5 percent at the pressure levels for tests 2, 3, and 4, respectively (see table I). Inasmuch as the same nozzle blocks were used for both tunnel configurations, the upstream turbulence intensities could be used as a measure of the test-section turbulence level. Readings of the apparent intensity were also taken in the test section for configuration B. These intensities were 3.5 percent for test 2 and 1.0 percent for tests 3 and 4. The apparent intensities should be regarded as qualitative. Measurements of a preliminary nature revealed the presence of a peak in the energy-spectrum curve below about 40 cycles per second for both configurations. The frequency range of the peak suggests that the indicated turbulence intensities include the effects of stream disturbances other than turbulence which could arise from tunnel piping resonances or from the compressor system. That the amplitude of the peak was much lower, however, for configuration B, reflects the greater effectiveness of the damping-screen arrangement. Operating conditions for the various tests are summarized in table I.

The Ames cone described in reference 8 was available for test 1 only. The Lewis cone, which was used as the test model for tests 2 to 4, is similar to the Ames cone in regard to included angle, 10°; wall thickness, 0.032 inch; material, 18-8 stainless-steel alloy; and surface finish (maximum roughness less than 15 microin.); but it is $18\frac{7}{16}$ inches long instead of 15 inches, and the internal dimensions differ somewhat near the apex, as shown in figure 1. The two cones also differ in the number and spacing of the constantan thermocouple wires soldered into holes in the shell. It is believed that results obtained from either cone are comparable. Under equilibrium conditions, the surface of these models closely simulates the ideal adiabatic surface, in view of the stagnant air in the cone interior and of the thin walls and relatively poor conductivity of stainless steel.

A single stainless-steel wire connected to the base of the cone completes the thermocouple circuit for each cone. Although the instruments used with the thermocouples have accuracies of $\pm 0.25^{\circ}$ F, repeatability of temperature measurements during a temperature survey was probably $\pm 0.5^{\circ}$ F because of gradual changes in tunnel stagnation temperature. The change in stagnation temperature during the schlieren observations to be described was about 3° F.

Figure 2 shows a typical spark-schlieren photograph of the cone boundary layer taken at an exposure of about 1 microsecond. The point at which the boundary-layer flow first appears to change from laminar to turbulent flow is indicated as the transition point. The location of the transition point was obtained from many high-speed schlieren

photographs taken at approximately uniform intervals of 20 seconds. The numbers of photographs used for tests 1 to 4 were 183, 367, 272, and 595, respectively. These numbers were dictated by operational limitations.

RESULTS AND DISCUSSION

Statistical Results

The schlieren observations of the transition-point location were arranged in the order of increasing distances from the cone apex and numbered. The total number of times transition occurred upstream of a given point x on the cone was thus obtained. Division of this number by the total number of cases yields the proportion of the time for which transition occurs upstream of a specified point. This function $G(x)$ is known as the statistical distribution function pertaining to that location (ref. 14). A second statistical quantity, the probability density $g(\eta)$, may be defined. The function $g(\eta)\,d\eta$ represents the fraction of the time that the transition point is located between η and $\eta + d\eta$. The relation between the two functions is given by

$$G(x) = \int_{\alpha}^{x} g(\eta)\,d\eta$$

(A list of symbols used will be found in appendix A.)

The statistical distribution functions obtained for tests 1 to 4 are shown by the individual points in figure 3. It is of interest to compare these with the normal, or Gaussian, distribution functions

$$G(x) = \frac{h}{\sqrt{\pi}} \int_{-\infty}^{x} e^{-(\eta-\mu)^2 h^2}\,d\eta$$

where μ is the arithmetic mean and h is the precision measure. The precision measure h and the standard deviation σ are related as $2h^2\sigma^2 = 1$. The arithmetic means of the experimental distributions are obtained from the discrete analog of the relation

$$\mu = \int_{\alpha}^{\beta} \eta\, g(\eta)\,d\eta$$

where $g(\eta) = 0$ when $\eta < \alpha$ and when $\eta > \beta$ (see appendix B). The precision measures are then similarly obtained from the relation

$$2h^2 = \int_{\alpha}^{\beta} (\eta - \mu)^2 \, g(\eta) \, d\eta$$

The physical meaning of the arithmetic mean is well known. The larger the slope of the central portion of the distribution function, the larger the precision measure. The quantities μ and h for the various tests are listed in table I. The normal, or Gaussian, distribution functions corresponding to these listed values of μ and h are plotted as the solid curves in figure 3. The experimental distribution functions for tests 3 and 4 appeared to fit so closely to the normal form that the values of μ and h obtained from the data for these particular tests were adjusted for best fit to the normal by the least-squares technique described in appendix B. These adjusted values are $\mu = 9.93$, $h = 1.336$ and $\mu = 8.02$, $h = 1.250$ for tests 3 and 4, respectively.

The effect of lowered stream turbulence in reducing the width of the transition zone ($\alpha < \eta < \beta$) is quite apparent from figure 3(a), which shows the distribution functions obtained with the high- and low-turbulence-level settling chambers at constant test-section Reynolds number. Both distributions extend upstream from essentially the same location - about $11\frac{1}{2}$ inches from the apex. The effect of increasing the stream-turbulence level in these tests was to increase the probability that the instantaneous transition point (in the sense of fig. 2) would be found farther upstream of the $11\frac{1}{2}$-inch station. Thus, it would appear that the farthest downstream position at which an instantaneous transition is observed is least sensitive to stream-turbulence level and presumably represents to first order the transition-point location for minimum instantaneous stream turbulence. A transition Reynolds number using as characteristic length the distance farthest downstream from the apex at which an instantaneous transition is observed might approximate the Reynolds number of transition for free flight. Such a speculation would require additional experimental verification.

The distribution functions obtained with the low-turbulence settling chamber (configuration B) are shown in figure 3(b). The primary effect of changing the test-section Reynolds number is to translate rather than to spread out the distribution functions. The changes in precision measure h listed for these tests in table I do not indicate any consistent trend with either Reynolds number or turbulence level.

The close approximation of the distribution functions of tests 3 and 4 to the normal distribution has already been mentioned. The departure of the test 1 distribution function from the normal form would indicate that the transition process, although random, is being influenced by some nonrandom disturbances. Such disturbances could very well stem from the tunnel piping resonances and from the compressor system mentioned in connection with spectrum measurements. Also, with the large extension of the transition zone occurring at high free-stream turbulence levels, any three-dimensional model effects stemming from the change of body radius with axial distance would be accentuated.

Recovery-Factor Distributions

Temperature-recovery-factor distributions obtained are shown in figures 4 and 5. The readings of the farthest downstream thermocouple on each of the two cones are believed to be influenced by heat transfer from the mounting strut and therefore should not be considered. The large deviation from the faired line of the recovery factors obtained in test 1 at stations $4\frac{1}{2}$, 5, 7, and $8\frac{1}{2}$ inches from the cone apex (fig. 4) are attributed to malfunctioning of the corresponding thermocouples, inasmuch as this pattern was also obtained at other Reynolds numbers with the same installation.

Figure 4 compares the effect of different stream-turbulence levels (as indicated by the apparent rms intensity of the longitudinal velocity fluctuations) upon the distribution of recovery factor for constant test-section Reynolds number, the change in turbulence level being accomplished by changing settling-chamber configurations. Figure 5 compares the effect of test-section Reynolds number upon recovery-factor distribution for a fixed settling-chamber configuration (configuration B) and presumably fixed turbulence level. Actually, as may be seen from table I, operation of the compressor system at different pressure levels causes some change in the turbulence level.

Within the limits of experimental accuracy, it appears that changing the turbulence level or test-section Reynolds number has little, if any, effect upon the values of either the peak or turbulent recovery factor. The effect of lowering the turbulence level is to intensify the rate at which the recovery factor reaches its maximum value (fig. 4) and thereby to increase the transition Reynolds number defined as in reference 8 (indicated schematically in fig. 6) from about 1.4×10^6 to 3.2×10^6. The nominal transition region is thus broader for the high- than for the low-turbulence-level stream and corresponds closely to the trend observed on the statistical distribution functions. In view of the earlier discussion it can readily be seen that the transition Reynolds number defined in reference

8, which is weighted towards the upstream point of the distribution function, would be very sensitive to changes in stream turbulence. The effect of increasing the test-section Reynolds number has been to translate the recovery-factor distribution curve (fig. 5) towards the apex of the cone. For tests 3 and 4, the transition Reynolds number as defined in reference 8 remained constant at 3.2×10^6; for test 2, this Reynolds number was 2.8×10^6.

A study of the schlieren photographs indicated that, for tests 2 to 4, compression-expansion wave systems intersected the cone at stations $5\frac{1}{2}$, 10, and 12 inches from the apex. The results of a brief investigation to determine the effects of a compression-expansion wave system on the recovery-factor distribution are shown in figure 7. Cellophane-tape strips 0.0025- and 0.005-inch thick and 0.75-inch wide placed on the tunnel wall generated the disturbance that, on the basis of schlieren observations, was clearly of greater strength than the wave systems already present in the flow. The results indicate that waves (generated by 0.005-in.-thick tape) intersecting the cone in the transition region do not greatly alter the recovery-factor distribution; whereas, upstream disturbances even of lower strength tend to move the transition region forward. Thus, it would appear that the recovery-factor distributions of tests 3 and 4 were less influenced than that of test 2 by the wave intersections. Presumably a similar conclusion would apply to the corresponding distribution functions.

Instantaneous Temperature-Recovery Factors

The temperature-recovery-factor distributions of references 8 and 9 as well as those just presented are time-averaged. The relation of the statistical distribution functions and the time-averaged recovery factors may be determined by means of a simple hypothesis. For clarity, reference will be made to temperature rather than to recovery factor.

An instantaneous temperature distribution that moves with the transition-point location and is unaffected by translation of the transition point is postulated. The random movement of the transition point is specified by a statistical distribution function $G(x)$ or, equivalently, a probability density function $g(\eta)$. Thus, when the transition point is located at a distance η from the cone apex, a thermocouple at a distance x from the apex is subjected to the instantaneous temperature $\theta(x - \eta)$ for $g(\eta)\, d\eta$ percentage of the time. The function $\theta(x - \eta)$, as shown in appendix B, has its maximum value at $x - \eta = 0$. Summing over all positions of the transition-point location gives the time-averaged temperature at the thermocouple:

$$\overline{T}(x) = \int_{\alpha}^{\beta} \theta(x - \eta)\, g(\eta)\, d\eta \qquad (1)$$

In the formulation of equation (1) the function $\theta(x - \eta)$ immediately upstream of the observed transition point need not be the laminar value. If the laminar value of the surface temperature is subtracted from both members of equation (1), there results

$$T(x) = \int_{\alpha}^{\beta} \Theta(x - \eta)\, g(\eta)\, d\eta \qquad (2)$$

where $T(x) \equiv \overline{T}(x) - \theta_L(x)$ and $\Theta \equiv \theta(x - \eta) - \theta_L(x)$. By a similar technique, equation (1) may be converted to recovery factors giving

$$\overline{r}(x) = \int_{\alpha}^{\beta} r_I(x - \eta)\, g(\eta)\, d\eta \qquad (3)$$

where $\overline{r}$ is the time-averaged recovery factor and r_I is the instantaneous recovery factor.

The iteration procedure used to obtain $\Theta(x - \eta)$ when $T(x)$ and $g(\eta)$ are known is described in appendix B. The temperature θ_L was taken as the temperature indicated by the thermocouple nearest the cone apex, and the instantaneous temperature distributions $\Theta(x - \eta)$ were obtained for tests 3 and 4. The sixth-iteration distributions converted to temperature-recovery factor are shown in figure 8. For tests 3 and 4, the maximum deviations in the derived mean temperatures obtained from the Θ-distributions of figure 8 and the appropriate probability densities are 0.30° F at $x = -2.0$ and 0.58° F at $x = -0.5$. The deviations at other points are for the most part 0.1° F or less.

Even though, in principle, equation (1) has a unique solution for $\Theta(x)$, many Θ distributions can be found which, with a given probability density distribution $g(\eta)$, will yield a time-averaged temperature distribution $T(x)$ within the accuracy of the temperature measurements. These alternative values of Θ oscillate about a mean curve that closely conforms to the corresponding Θ-distribution of figure 8. Thus, the precise form of Θ cannot be inferred without greater accuracy of the experimental data.

The instantaneous recovery-factor distributions retain the general characteristics of the mean distributions but show a steeper rise and higher peak recovery factor. In a time-dependent flow, the mixing to be expected from large-eddy convective-type transfer could disturb the proportion of heat and momentum transfer and lead to an increase in recovery factor. The subsequent levelling off of recovery factor to the value appropriate for fully turbulent flow suggests the physical picture of large eddies diffusing rapidly to form a turbulent flow.

It will be recalled that in the derivation of equation (1) the assumption was made that the instantaneous distribution is not affected by its position and rate of change of movement through the region of developing boundary layer. The differences between the two instantaneous distributions shown in figure 8 suggest that a more precise analysis might include some scaling factor to account for a Reynolds number effect. Such an analysis would require considerably more experimental data.

Emmons has proposed the concept (ref. 6) that transition on an aerodynamic surface results from the random appearance of turbulent sources that grow and eventually join to form a fully turbulent region. Such a transition process would be expected to produce many examples of turbulent flow followed downstream by laminar flow. The data of the present paper suggest that there is a relatively sharp change from laminar to turbulent flow with predominantly turbulent flow downstream. The occurrence in the free stream of eddies whose scale is large compared with the boundary-layer thickness would favor the probability of observing turbulent flow downstream of the transition point; the presence of predominantly small-scale eddies would, on the other hand, increase the probability of observing multiple transition points.

A study of the schlieren photographs from test 3 indicates that about 2 percent of the cases (6 pictures in 272) show, as in figure 9, the obvious presence of more than one transition point. Thus, while the growth of turbulent spots that were so evident on Emmons' water-table experiments is not precluded, the evidence from the schlieren photographs indicates that such a transition mechanism did not predominate here. A possible inference would be that the scale of eddies in the tunnel air stream was large compared with the boundary-layer thickness.

A rapidly fluctuating transition point followed downstream by turbulent flow would explain in part, as does also the growth of turbulent spots, the apparent bursts of turbulence indicated by a hot-wire probe located in the transition zone. It should be recognized, however, that the hot-wire probe would also record the influence of relatively large-scale eddies that are expected to form at transition.

CONCLUDING REMARKS

The experimentally determined statistical distribution functions defining the transition-point location are markedly affected by stream-turbulence level, their axial extent being broad for high turbulence and narrow for low turbulence. The data suggest that the transition-point location for conditions of minimum instantaneous stream turbulence would correspond closely to the farthest observable downstream point on a distribution function obtained in a turbulent stream. The axial spread of the transition region indicated by measurement of local recovery-factor distributions, in general, corresponds to that of the distribution function. It would appear that the primary effect of changing test-section Reynolds number is to translate rather than to spread out or to sharpen the recovery-factor distribution curves.

The data suggest a simple concept wherein the flow is postulated to change sharply from laminar to turbulent flow, this instantaneous flow field moving randomly in the longitudinal direction about an aerodynamic surface. The measured recovery factors and distribution functions were utilized to calculate the hypothesized instantaneous recovery-factor distribution for several Reynolds numbers. An extension of the present investigation to include effects of Mach number upon transition appears warranted.

Lewis Flight Propulsion Laboratory
National Advisory Committee for Aeronautics
Cleveland, Ohio, November 2, 1953

APPENDIX A

SYMBOLS

The following symbols are used:

$G(x)$ distribution function of x; probability that $x_1 < \eta \leq x_2$ is given by $G(x_2) - G(x_1) \equiv \int_{x_1}^{x_2} g(\eta)\, d\eta$

$g(\eta)$ probability density of η

h precision measure of distribution function related to standard deviation as $\frac{1}{h\sqrt{2}}$ defined by eq. (B11)

N total number of observations

q local stream dynamic pressure

$\bar{r}$ time-averaged temperature-recovery factor

r_I instantaneous temperature-recovery factor

$\bar{T}$ time-averaged surface temperature

T time-averaged surface-temperature increment above laminar temperature

x position variable measured from cone apex along a ray

α upstream limit of transition-point movement, $g(\eta) = 0$ for $\eta < \alpha$

β downstream limit of transition-point movement, $g(\eta) = 0$ for $\eta > \beta$

Δ increment in function value between successive approximations

ε defined by eq. (B12)

ζ defined in appendix B in connection with eq. (B15)

η variable specifying location from cone apex of instantaneous transition point

θ instantaneous surface temperature

Θ instantaneous surface-temperature increment above laminar temperature

μ arithmetic mean as defined in eq. (B10)

Subscripts:

L laminar

n order of approximation as used in appendix B

APPENDIX B

MATHEMATICAL PROCEDURES

By Hugo Heermann

Fitting of Distribution Functions

In order to find a solution of the integral equation

$$T(x) = \int_{\alpha}^{\beta} \Theta(x - \eta)\, g(\eta)\, d\eta \tag{B1}$$

it is necessary to process the data in such a way that the probability density $g(\eta)$ assumes a satisfactory mathematical form. The difficulties involved and the means of overcoming them are explained herein.

At p distinct points $x_1, x_2, x_3, \ldots x_p$ transition was observed to occur $n_1, n_2, \ldots n_p$ times, respectively. Thus, each $n_i \geq 1$. The total number of times transition was observed to occur is N, where

$$N = \sum_{i=1}^{p} n_i \tag{B2}$$

A function $G(x)$ is defined for each $x = x_k (k = 1,2,3, \ldots p)$ by means of the relation

$$G(x_k) = \sum_{i=1}^{i=k} n_i \tag{B3}$$

$G(x)$ is a step function that consists of steps of the heights $g(x_i)$, where

$$n_i = g(x_i)$$

at the jump points x_i. From equation (B3), with $n_i = g(x_i)$, it follows that

$$G(x_k) = \sum_{i=1}^{k} g(x_i) \tag{B4}$$

or

$$G(x_k) - G(x_{k-1}) = g(x_k) \tag{B5}$$

When $G(x)$ is differentiable, the continuous analogs of equations (B4) and (B5) are

$$G(x) = \int_{\alpha}^{\beta} g(\eta)\, d\eta \tag{B6}$$

and

$$\frac{dG(x)}{dx} = g(x) \tag{B7}$$

However, since $G(x)$ is a step function, the difficulties involved in evaluating $g(x)$ by equation (B7) are evident. Consequently, some other procedure had to be devised.

After the discontinuous distribution function $G(x)$ for tests 3 and 4 was plotted, it was observed that these distributions appeared to be nearly normal. This means that for an appropriate choice of the parameters μ and h, $G(x)$ can be approximated by

$$G(x) \cong \frac{h}{\sqrt{\pi}} \int_{\alpha}^{x} e^{-h^2(\eta-\mu)^2}\, d\eta \tag{B8}$$

Thus, if $G(x)$ could be put in the form (B8), it could be immediately inferred that

$$g(x) \approx \frac{h}{\sqrt{\pi}}\, e^{-h^2(x-\mu)^2} \tag{B9}$$

The decision that the differentiable distribution function that best fits the data is a normal distribution means that some procedure must be evolved for evaluating the parameters μ and h. When there is a very large number of observations, these parameters are usually obtained from the relations

$$\left.\begin{aligned} \mu &= \frac{\sum_{i=-\infty}^{i=+\infty} x_i g(x_i)}{N} \\ \mu &= \int_{-\infty}^{+\infty} \eta g(\eta)\, d\eta \end{aligned}\right\} \quad \begin{aligned} &\text{for discontinuous probability density functions} \\ &\text{for continuous probability density functions } g(x) \text{ for which } \int_{-\infty}^{+\infty} g(\eta)\, d\eta = 1 \end{aligned} \tag{B10}$$

$$\left.\begin{aligned} \frac{1}{2h^2} &= \frac{\sum_{i=-\infty}^{i=+\infty} (x_i - \mu)^2 g(x_i)}{N^2} \\ \frac{1}{2h^2} &= \int_{-\infty}^{+\infty} (\eta - \mu)^2 g(\eta)\, d\eta \end{aligned}\right\} \quad \begin{aligned} &\text{for discontinuous probability density functions} \\ &\text{for continuous probability density functions for which } \int_{-\infty}^{+\infty} g(\eta)\, d\eta = 1 \end{aligned} \tag{B11}$$

In view of the statistically small samples involved in tests 3 and 4, it was thought that the μ and h obtained from equations (B10) and (B11) might not be satisfactory. It was therefore decided to choose μ and h so that $\frac{h}{\sqrt{\pi}} \int_{\alpha}^{x} e^{-(\eta-\mu)^2 h^2}\, d\eta$ would approximate the experimental $G(x)$ in the sense of least squares in the observed range. Thus, if

$$\varepsilon(\mu,h) = \int_{\alpha}^{\beta} \left[G(x) - \frac{h}{\sqrt{\pi}} \int_{\alpha}^{x} e^{-(\eta-\mu)^2 h^2}\, d\eta \right]^2 dx \tag{B12}$$

then μ and h are to be found so that $\varepsilon(\mu,h)$ is a minimum. This leads to the two equations

$$\frac{\partial \varepsilon}{\partial h}(\mu,h) = 0 \tag{B13}$$

$$\frac{\partial \varepsilon}{\partial \mu}(\mu,h) = 0 \tag{B14}$$

When the values of μ and h predicted by equations (B10) and (B11) are used as initial approximations, equations (B13) and (B14) are solved with use of finite summations by Newton's method (ref. 15). With μ and h determined in this manner, a satisfactory form for the probability density is obtained through use of equation (B9).

Solution of Integral Equation

The problem is to find a function $\Theta(x)$ that satisfies the integral equation of the first kind with fixed limits:

$$T(x) = \int_{\alpha}^{\beta} \Theta(x - \eta)\, g(\eta)\, d\eta \tag{2}$$

In order to obtain the physical significance of Θ, as implied in the text, the argument must be replaced by $x - \eta$. If it is assumed that for the given numerical data there exists a continuous function $\Theta(x)$ which satisfies this equation, then by the mean-value theorem there exists a function $\zeta(x)$ for which $\alpha < \zeta(x) < \beta$, so that

$$T(x) = \Theta\left[x - \zeta(x)\right] \int_{\alpha}^{\beta} g(\eta)\, d\eta \tag{B15}$$

or, since

$$\int_{\alpha}^{\beta} g(\eta)\, d\eta = 1$$

then

$$T(x) = \Theta\left[x - \zeta(x)\right] \tag{B16}$$

where

$$\alpha < \zeta(x) < \beta$$

When h is very large, much more can be said about $\zeta(x)$. From equations (1.18.1) and (1.16.4) of reference 16 it can be shown that

$$\lim_{h\to\infty}\left[\frac{h}{\sqrt{\pi}}\int_{-\infty}^{\infty} T(x+\mu-\eta)e^{-h^2(\eta-\mu)^2}\,d\eta\right] = T(x)$$

When equation (B1) is rewritten in the form

$$\frac{h}{\sqrt{\pi}}\int_{\alpha}^{\beta} \Theta(x-\eta)e^{-h^2(\eta-\mu)^2}\,d\eta = T(x)$$

comparison of these equations indicates that, for large h, a good initial approximation to the solution of equation (B1) is

$$\Theta_0(x) = T(x+\mu) \tag{B17}$$

Thus, when h is very large, $\zeta(x) \approx \mu$. By experiment it was found that, even when h is not large, (B17) still furnishes a reasonable approximation to the solution of (B1). In fact, the maximum value of

$$\left|T(x) - \int_{\alpha}^{\beta} \Theta_0(x-\eta)g(\eta)\,d\eta\right| \tag{B18}$$

occurred at $x \approx \mu$, and for increasing values of x larger than μ, the difference given by equation (B18) decreases and finally becomes zero. A similar remark applies when $x < \mu$ and for decreasing values of x. Thus, the maximum errors involved in assuming $\Theta_0(x) = T(x+\mu)$ to be a solution occurred in a neighborhood of the point $x = 0$, as in the following sketch:

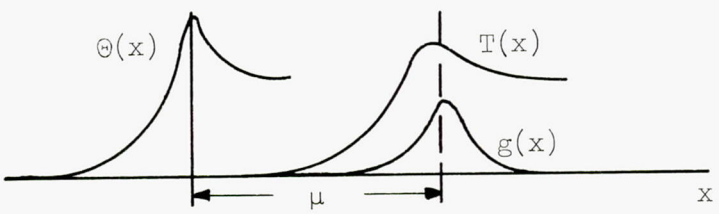

In order to improve on the initial approximation (B17), suppose that $\Theta_1(x)$ is a solution of (B1), and let

$$\Theta_1(x) = \Theta_0(x) + \Delta_0(x)$$

Then

$$T(x) = \int_\alpha^\beta \Theta_0(x - \eta)g(\eta)\, d\eta + \int_\alpha^\beta \Delta_0(x - \eta)g(\eta)\, d\eta$$

By the mean-value theorem,

$$T(x) = \int_\alpha^\beta \Theta_0(x - \eta)g(\eta)\, d\eta + \Delta_0\left[x - \zeta_1(x)\right]$$

where $\alpha < \zeta_1(x) < \beta$. From (B18) it follows that the maximum value of

$$\left|\Delta_0\left[x - \zeta_1(x)\right]\right|$$

occurs at $x = \mu$. This suggests the choice

$$\zeta_1(x) = \mu$$

so that

$$\left|\Delta_0(x - \mu)\right|$$

will be largest when $x = \mu$.

A method of successive approximations defined in accordance with the following is thereby indicated:

$$\Theta_0(x) = T(x+\mu)$$

$$\Theta_1(x) = \Theta_0(x) + \Delta_0(x); \qquad \Delta_0(x - \mu) = T(x) - \int_\alpha^\beta \Theta_0(x - \eta)g(\eta)\, d\eta$$

. . . . . .

. . . . . .

$$\Theta_{n+1}(x) = \Theta_n(x) + \Delta_n(x) \qquad \Delta_n(x - \mu) = T(x) - \int_\alpha^\beta \Theta_n(x - \eta)g(\eta)\, d\eta$$

If $\Theta_n(x)$ tends uniformly in $-\infty < x < +\infty$ to a limit $\Theta(x)$

$$\Theta(x) = \lim_{n\to\infty} \Theta_n(x)$$

then $\Theta(x)$ will satisfy equation (B1).

In the computations the integration step size was taken as 0.25 inch. The spacing of the thermocouple being 0.5 inch, a smaller step size was not considered warranted.

REFERENCES

1. Pillow, A. F.: A Review of Hydrodynamic Stability and Its Bearing on Transition to Turbulent Flow in the Boundary Layer. Rep. A.35, Div. Aero., Council Sci. and Ind. Res., Melbourne (Australia), May 1945.

2. Lees, Lester, and Lin, Chia Chiao: Investigation of the Stability of the Laminar Boundary Layer in a Compressible Fluid. NACA TN 1115, 1946.

3. Lees, Lester: The Stability of the Laminar Boundary Layer in a Compressible Fluid. NACA Rep. 876, 1947. (Supersedes NACA TN 1360.)

4. Taylor, G. I.: Statistical Theory of Turbulence. V - Effect of Turbulence on Boundary Layer. Theoretical Discussion of Relationship Between Scale of Turbulence and Critical Resistance of Spheres. Proc. Roy. Soc. (London), vol. CLVI, no. A.888, ser. A, Aug. 17, 1936, pp. 307-317.

5. Roshko, Anatol: On the Development of Turbulent Wakes from Vortex Streets. NACA TN 2913, 1953.

6. Emmons, H. W.: The Laminar-Turbulent Transition in a Boundary Layer, Part I. Jour. Aero. Sci., vol. 18, no. 7, July 1951, pp. 490-498.

7. Emmons, H. W., and Bryson, A. E.: The Laminar-Turbulent Transition in a Boundary Layer. Proc. First U.S. Nat. Cong. Appl. Mech., June 1951, pp. 859-868.

8. Ross, Albert O.: Determination of Boundary-Layer Transition Reynolds Numbers by Surface-Temperature Measurements of a 10° Cone in Various NACA Supersonic Wind Tunnels. NACA TN 3020, 1953.

9. Stine, Howard A., and Scherrer, Richard: Experimental Investigation of the Turbulent-Boundary-Layer Temperature-Recovery Factor on Bodies of Revolution at Mach Numbers from 2.0 to 3.8. NACA TN 2664, 1952.

10. Coles, Donald: Direct Measurement of Supersonic Skin Friction. Jour. Aero. Sci., vol. 19, no. 10, Oct. 1952, p. 717.

11. Dryden, Hugh L.: Air Flow in the Boundary Layer Near a Plate. NACA Rep. 562, 1936.

12. Lee, Roland E.: Measurements of Pressure Distribution and Boundary-Layer Transition on a Hollow-Cylinder Model. NAVORD Rep. 2823, U. S. Naval Ord. Lab. (Maryland), Apr. 28, 1953.

13. Brinich, Paul F., and Diaconis, Nick S.: Boundary-Layer Development and Skin Friction at Mach Number 3.05. NACA TN 2742, 1952.

14. Arley, Niels, and Buch, K. Rander: Introduction to the Theory of Probability and Statistics. John Wiley & Sons, Inc., 1950.

15. Whittaker, E. T., and Robinson, G.: The Calculus of Observations. Third ed., Blackie and Son, LTD. (London), 1940, p. 90.

16. Titchmarsh, E. C.: Introduction to the Theory of Fourier Integrals. Second ed., Clarendon Press (Oxford), 1948.

TABLE I. - OPERATING CONDITIONS AND DISTRIBUTION-FUNCTION PARAMETERS

Configuration	Test number	Stagnation pressure, lb/sq in. abs	Stagnation temperature, °F	Test-section Reynolds number per foot	Indicated longitudinal turbulence intensity		Distribution-function parameters	
					Mach number 0.12 station, percent	Test section, percent	Arithmetic mean, μ (eq. (B10))	Precision measure, h (eq. (B11))
A	1	28.55	43.9	4.8×10^6	9.4	---	7.55	0.434
B	2	17.67	44.0	3.0×10^6	1.0	3.5	13.46	0.822
	3	29.01	46.0	4.8	.75	1.0	9.96	1.261
	4	40.11	48.8	6.6	.5	1.0	8.02	1.200

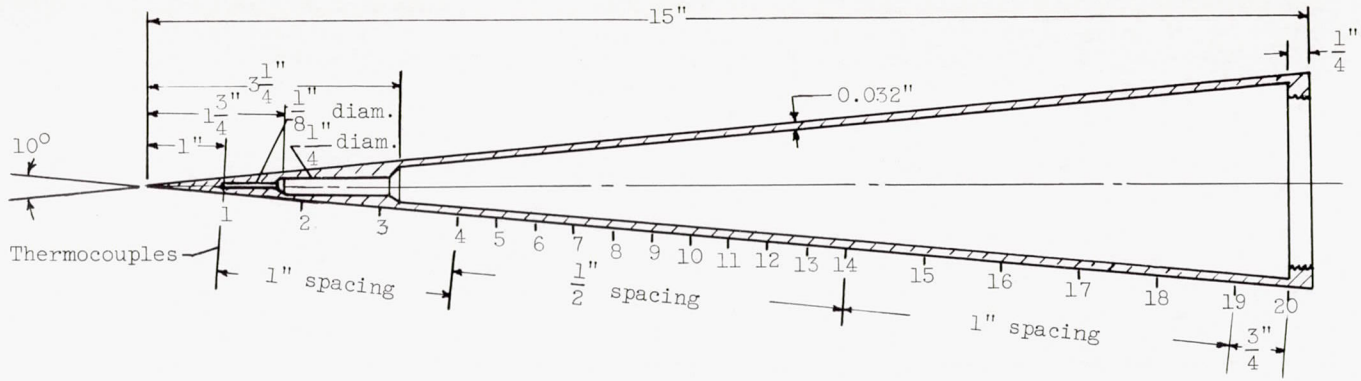

(a) Ames test cone.

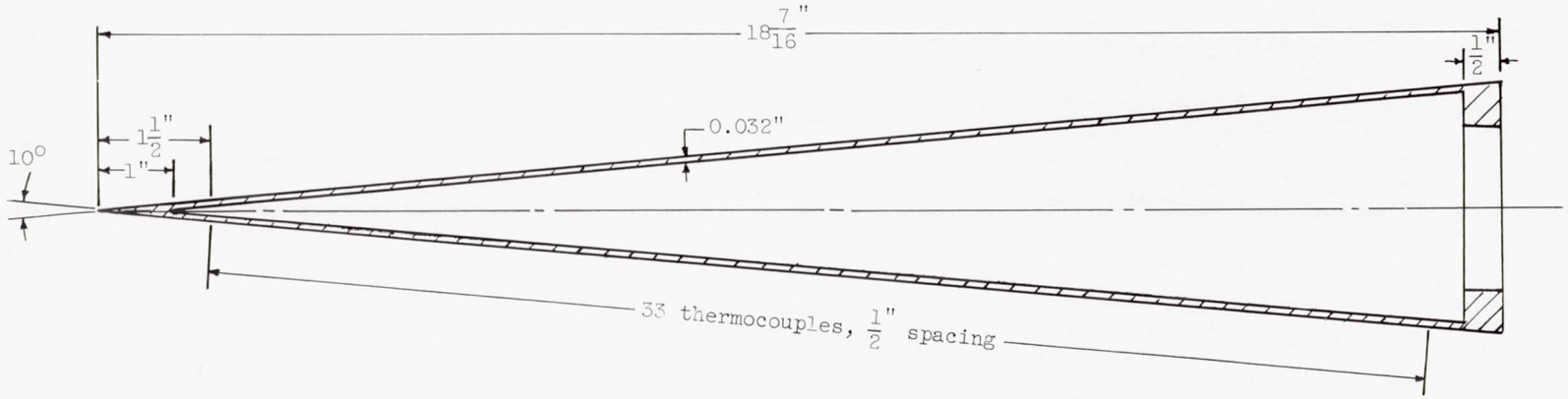

(b) Lewis test cone.

Figure 1. - Test-cone geometry and thermocouple locations.

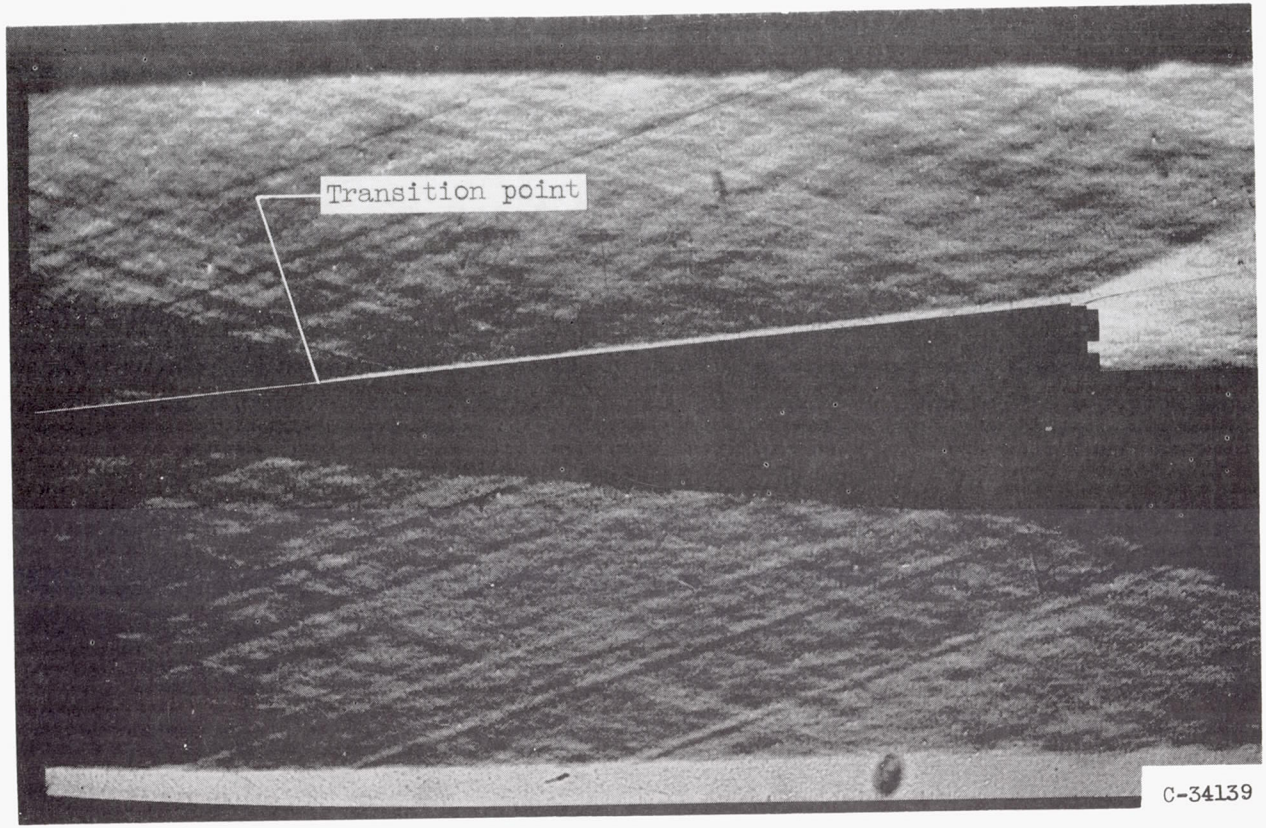

Figure 2. - Typical high-speed schlieren photograph showing cone boundary layer and apparent transition-point location. Exposure at approximately 1 microsecond.

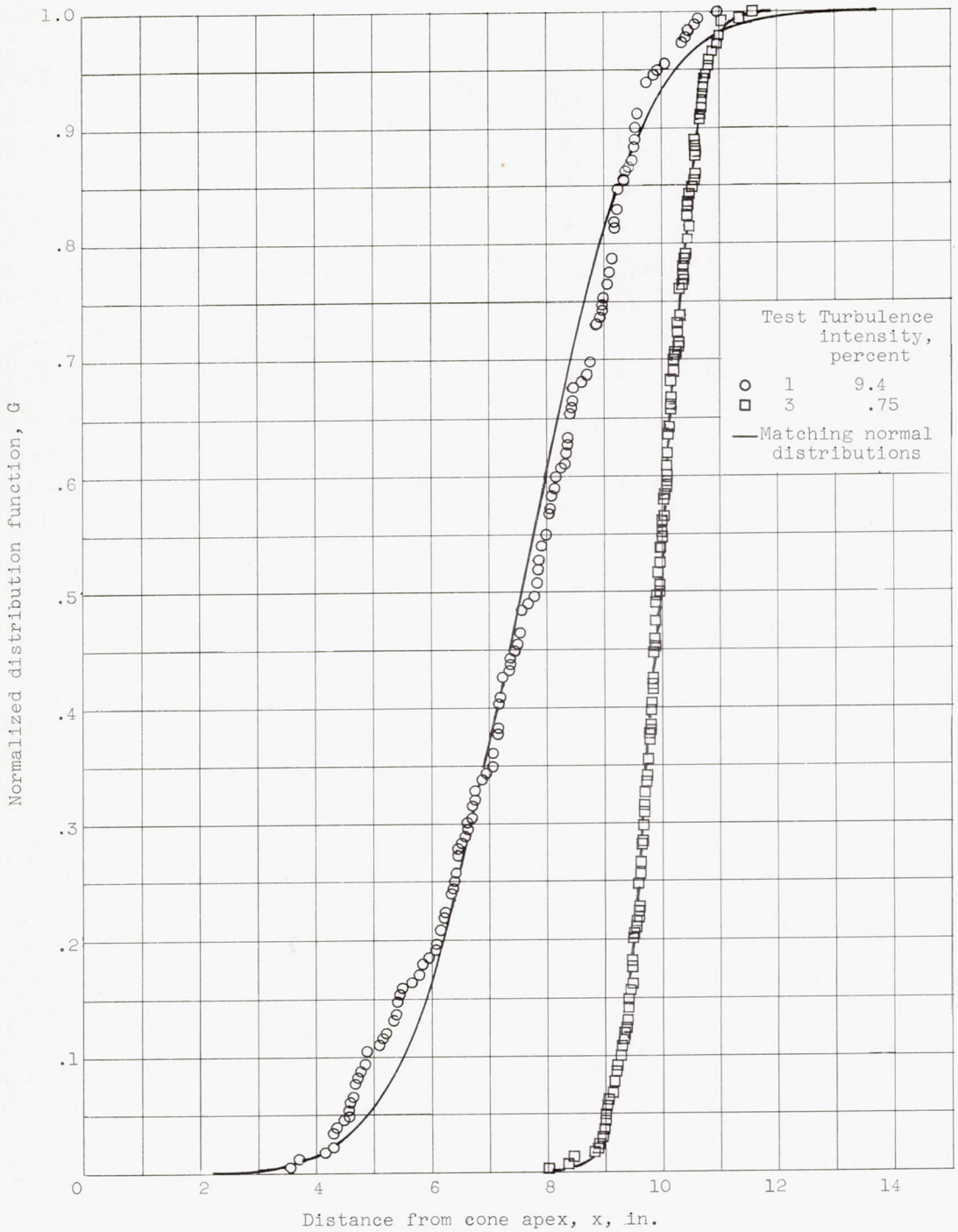

(a) Variable settling-chamber geometry and fixed test-section Reynolds number of 4.8×10^6 per foot.

Figure 3. - Distribution functions defining statistical location of transition point.

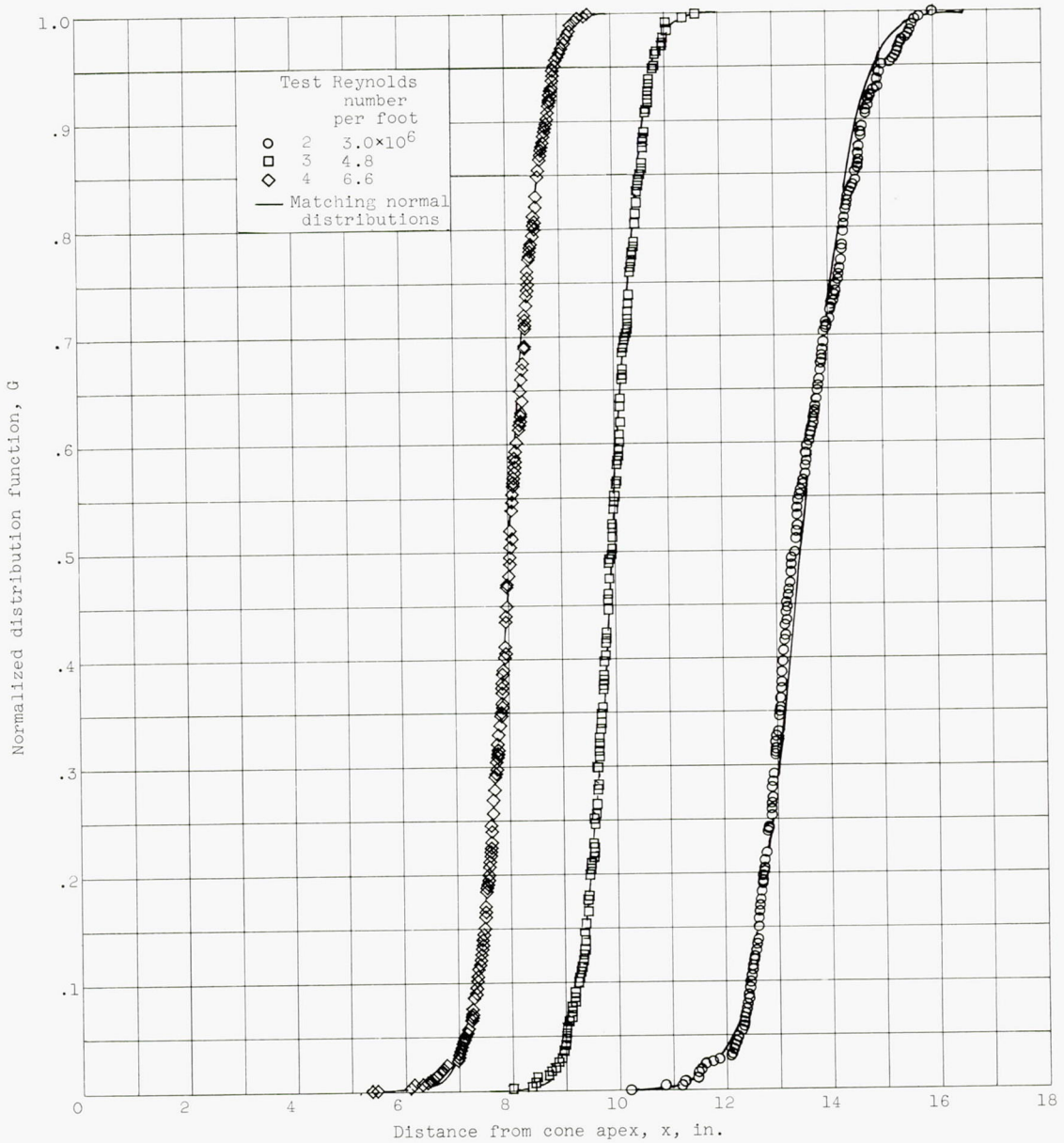

(b) Fixed settling-chamber geometry (configuration B) and variable test-section Reynolds number.

Figure 3. - Concluded. Distribution functions defining statistical location of transition point.

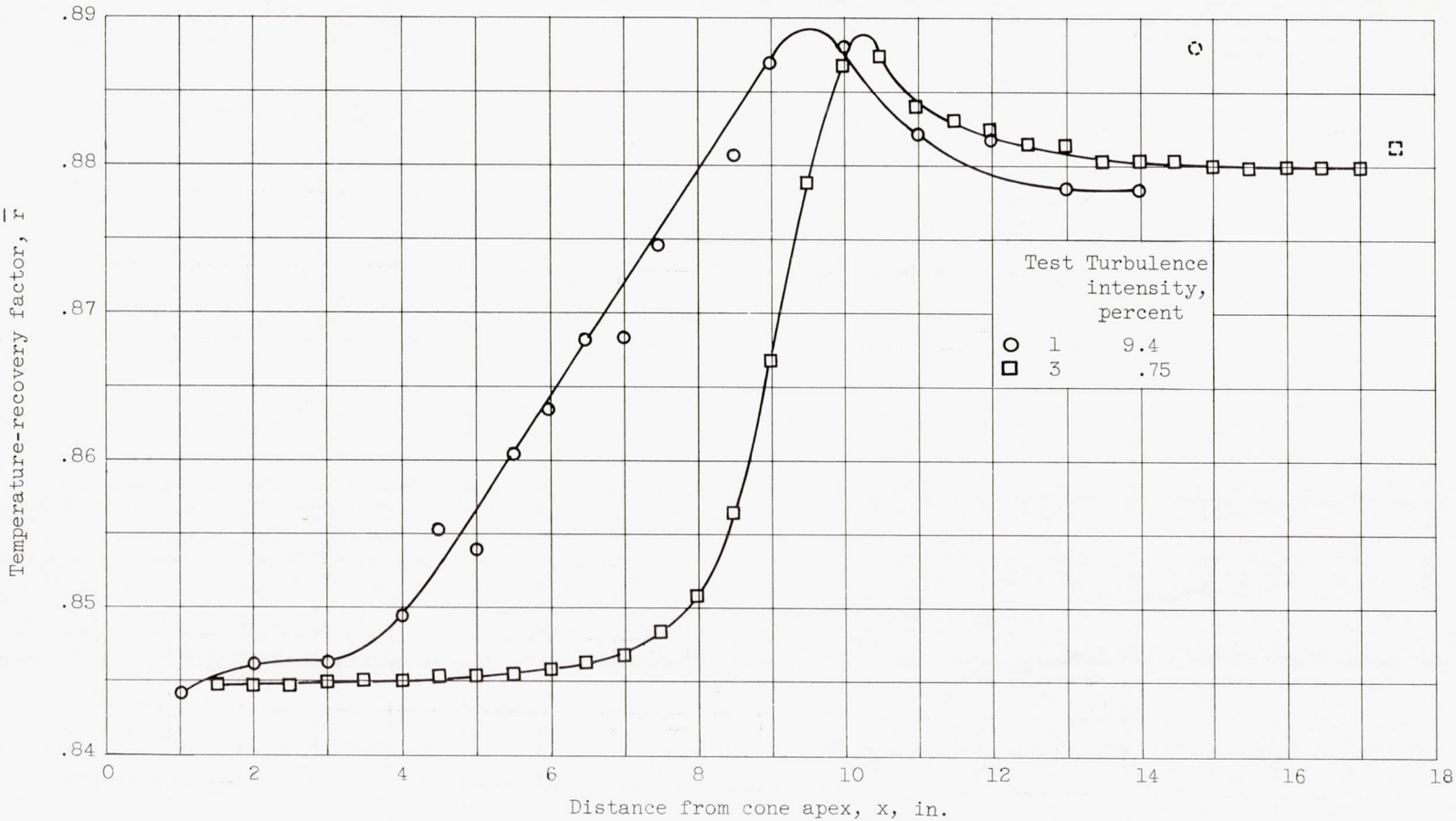

Figure 4. - Effect of varying settling-chamber geometry on temperature-recovery-factor distribution at fixed test-section Reynolds number of 4.8×10^6 per foot. Turbulence intensities measured in entrance section at Mach number 0.12.

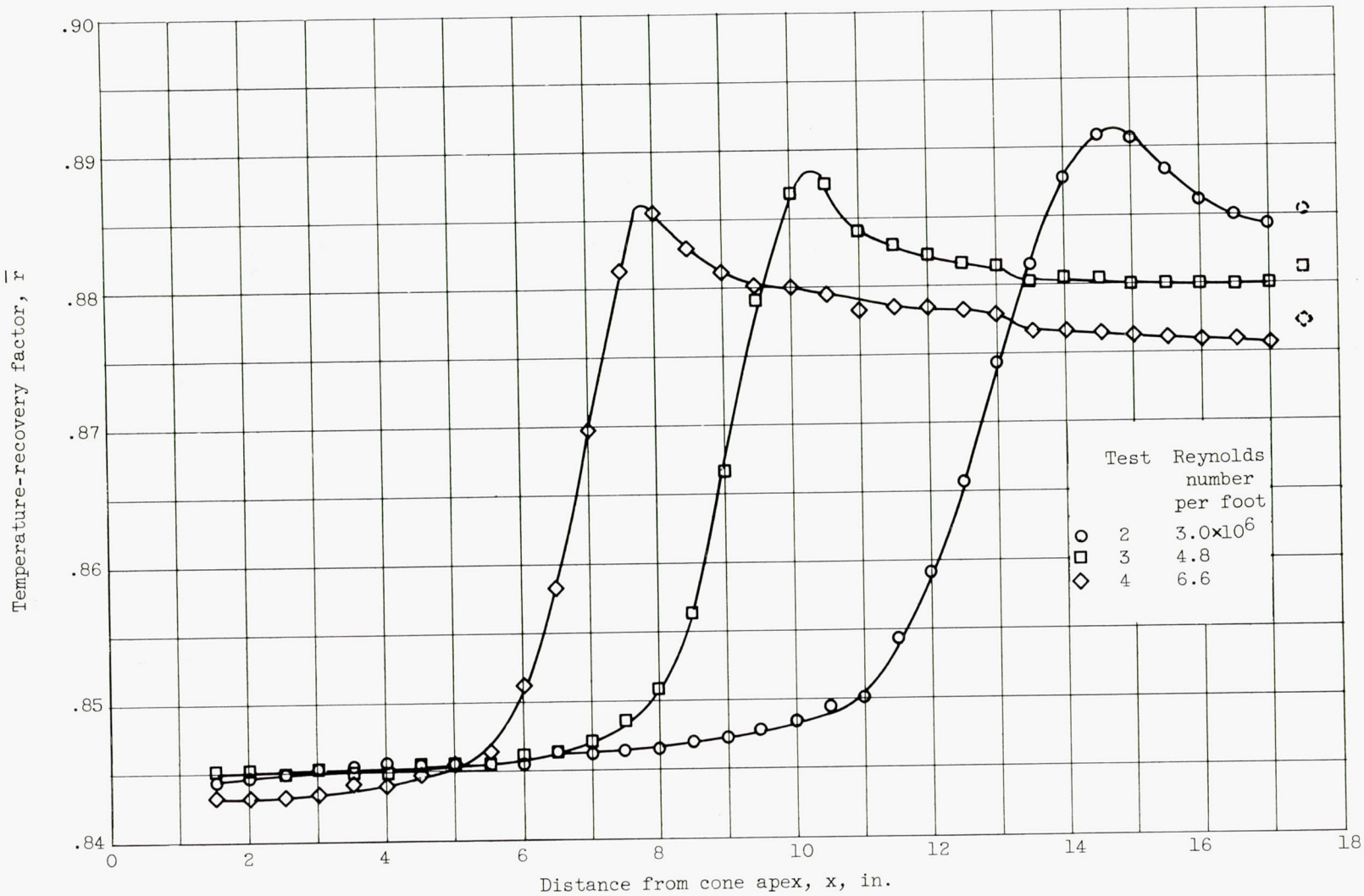

Figure 5. - Effect of test-section Reynolds number on temperature-recovery-factor distribution with fixed settling-chamber geometry (configuration B).

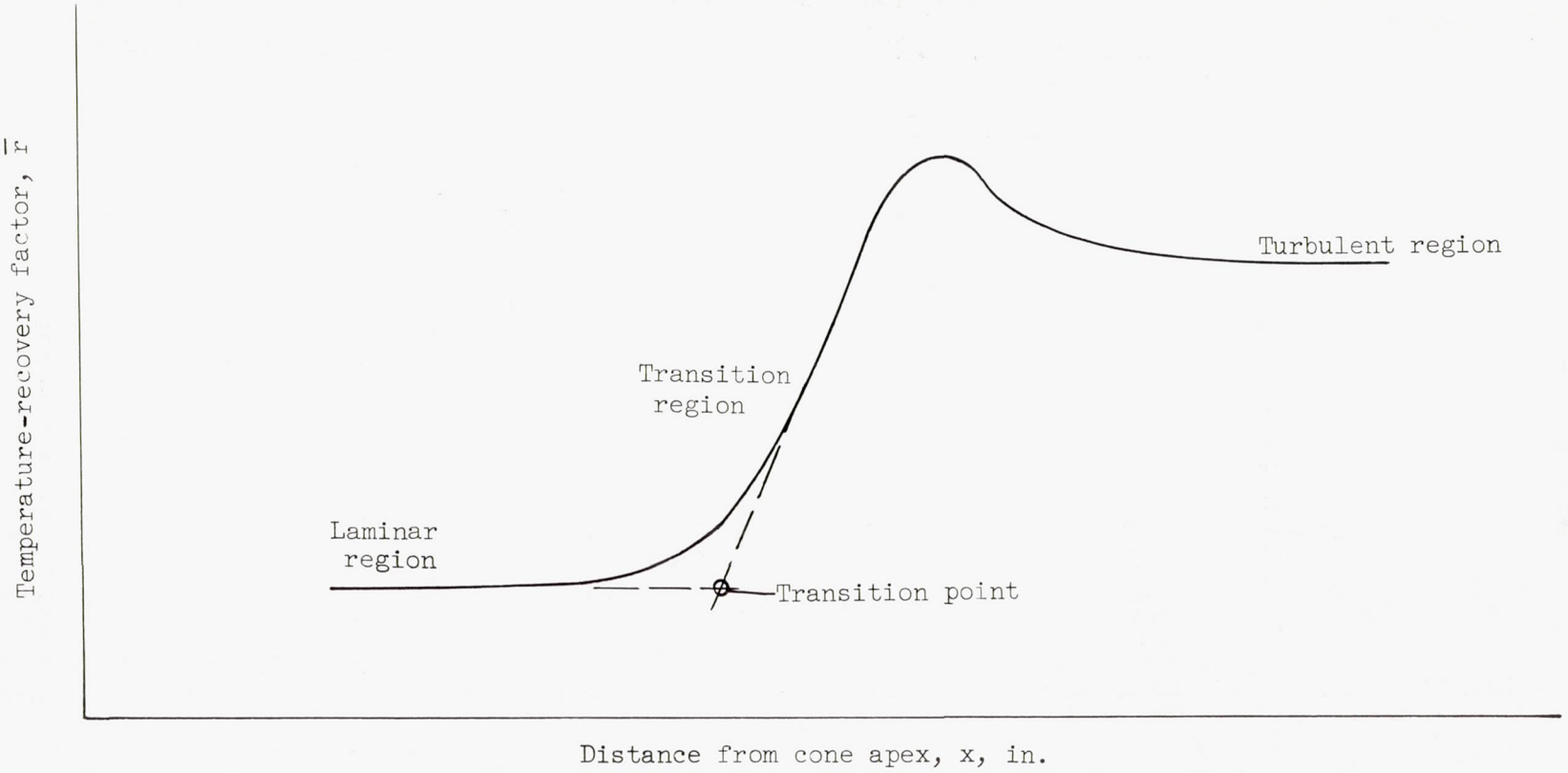

Figure 6. - Transition Reynolds number as determined from temperature-recovery factor according to method of reference 8.

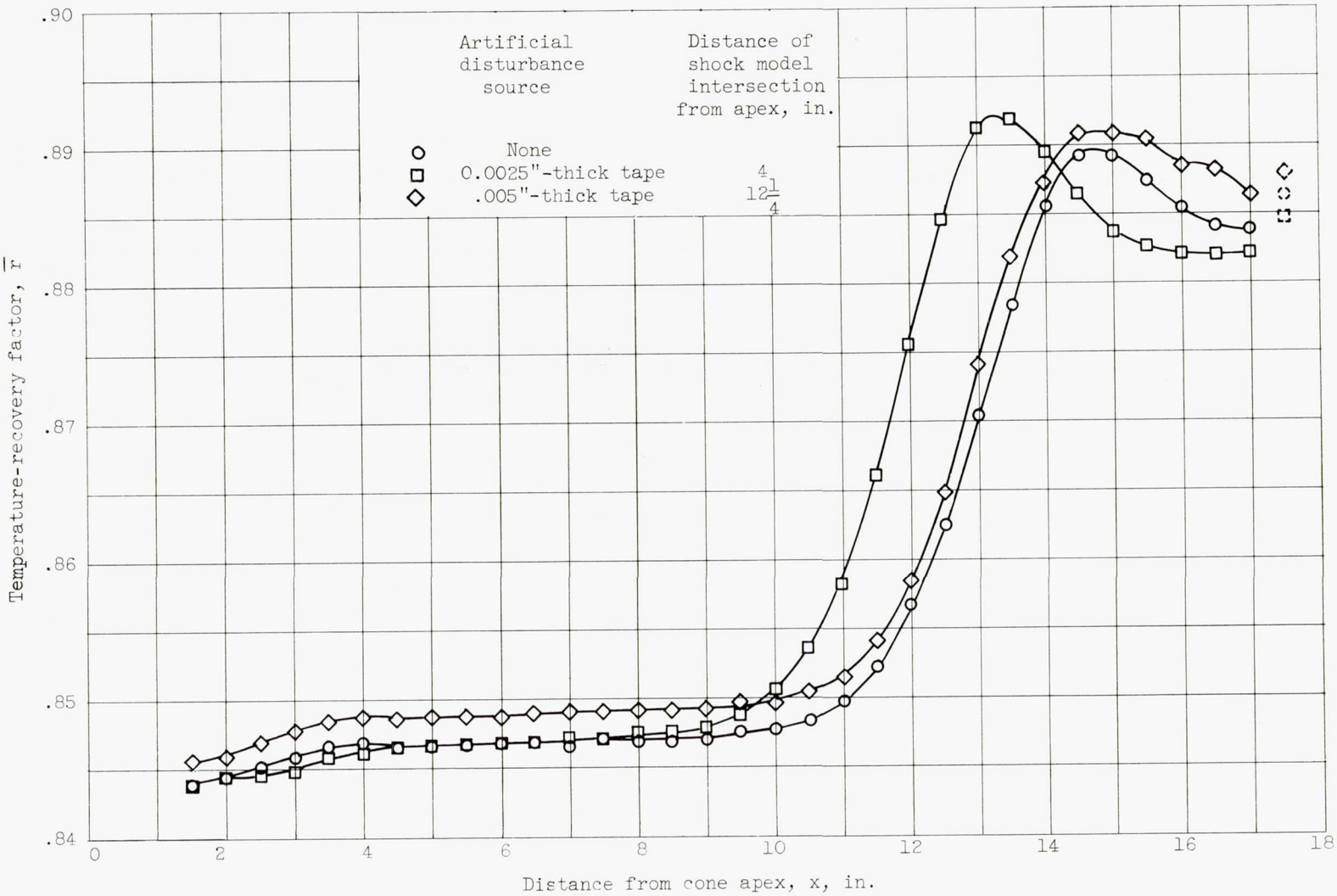

Figure 7. - Effect of compression-expansion wave system intersection on temperature-recovery-factor distribution. Wave system generated by 0.75-inch-wide cellophane-tape strips mounted on tunnel wall. Reynolds number per foot, 2.9×10^6.

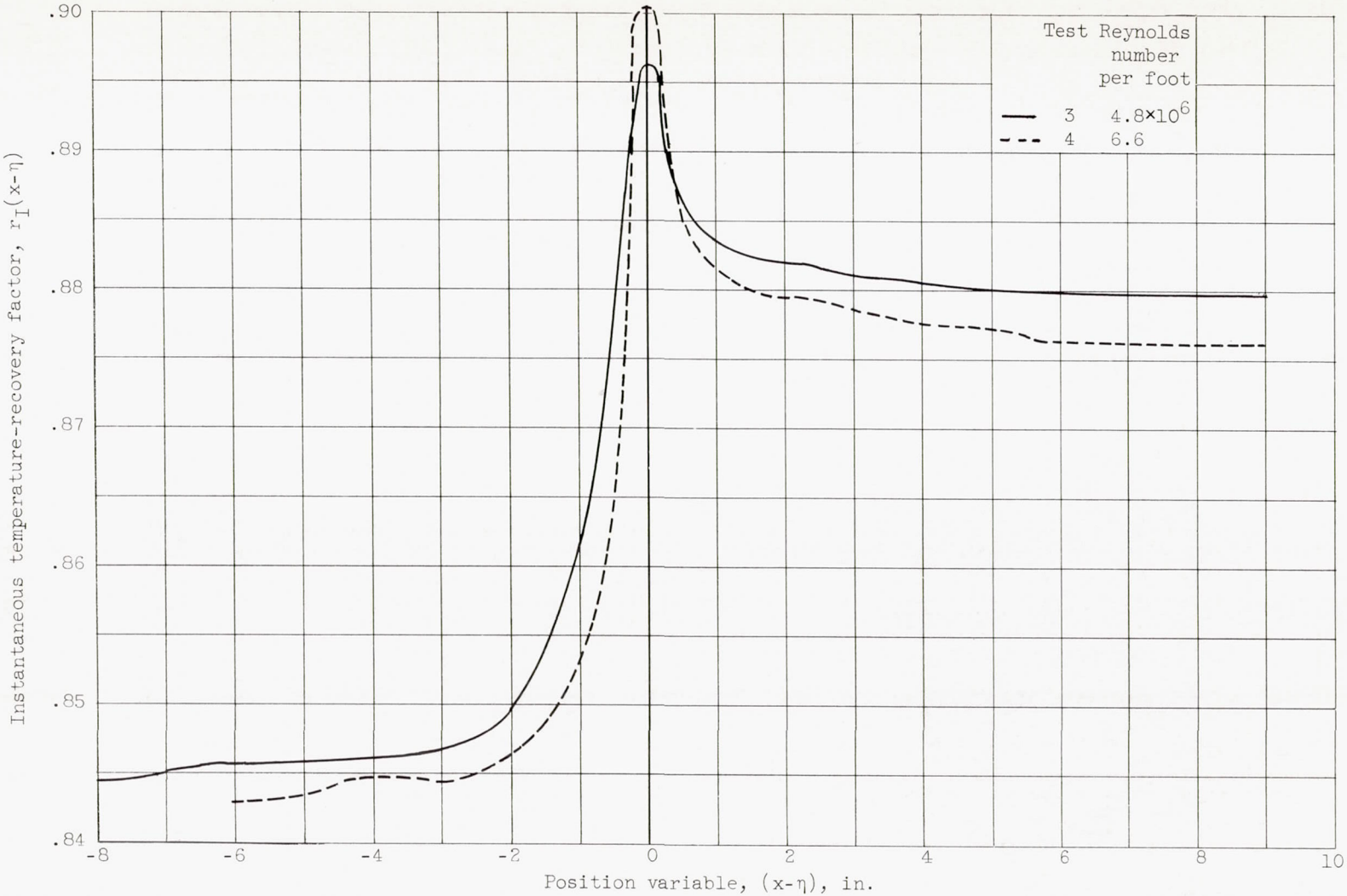

Figure 8. - Calculated instantaneous recovery-factor distributions for varying test-section Reynolds number and fixed test-section stream-turbulence intensity.

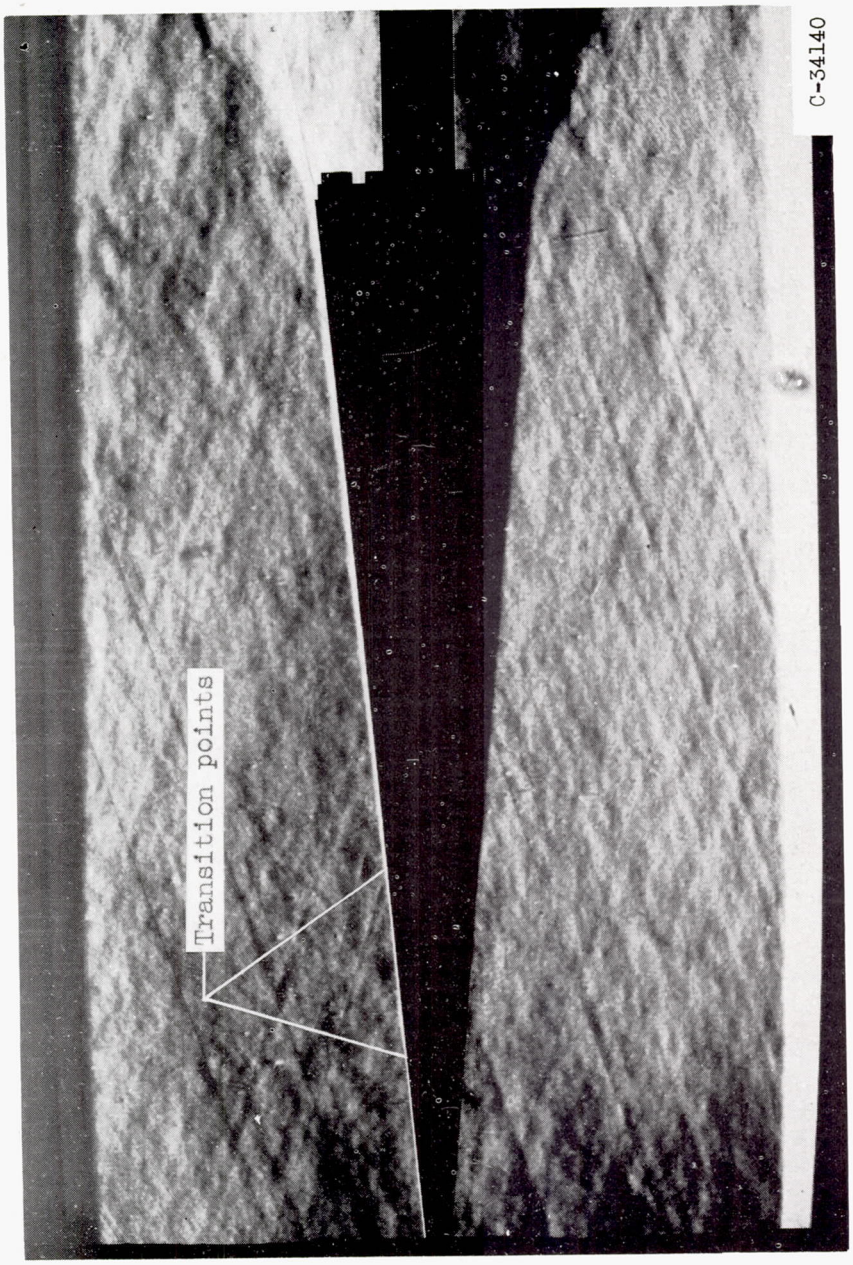

Figure 9. - High-speed schlieren photograph of cone boundary layer showing several apparent transition points.